A RECIPE TO GENERATE PHYSICALLY CONSISTENT EARTHQUAKE RUPTURE MODELS FOR GROUND MOTION PREDICTION

Mariagiovanna Guatteri [1], P. Martin Mai [2], Gregory C. Beroza [3]

[1] Swiss Reinsurance America, Armonk, NY 10504
[2] Institute of Geophysics, ETH Hoenggerberg, Zurich, CH-8093, Switzerland
[3] Department of Geophysics, Stanford, CA 94305-2215

Summary

Accurate predictions of the intensity and variability of ground motions from future large earthquakes depend strongly on our ability to simulate realistic models of the earthquake source. In order to make these simulations more accurate, we have developed a procedure to generate physically consistent earthquake rupture models. We term these models *pseudo-dynamic* because they are kinematic models that are designed to emulate important characteristics of fullly dynamic rupture models. The user-specified parameters to generate pseudo-dynamic rupture models are the earthquake magnitude and hypocenter, with the option of specifying the fault dimensions as well. We construct pseudo-dynamic models by first generating a slip distribution as a realization of a spatial random field that is consistent in its overall scaling and spatial variability with slip distributions observed in past earthquakes[*Mai and Beroza*, 2000; *Mai and Beroza,* 2002]. We compute the static stress drop associated with this slip distribution, which in turn is used to assign the temporal evolution of slip (rupture velocity, rise time, slip-velocity function) by applying a series of empirical relationships derived from the analysis of a set of spontaneous rupture models. A simple energy-budget calculation is used to discard source models that are not realizable as spontaneous ruptures.

Our approach is based on the findings of *Guatteri et al.* [2003], incorporating ideas developed by *Mai et al.* [2001] and *Guatteri et al.* [2002] for a source characterization that adequately describe the dynamics of rupture without having to do full dynamic simulations. The pseudo-dynamic approach circumvents the limits imposed by the extreme computational demand of generating fully dynamic rupture models for simulating multiple realizations of a scenario earthquake for strong-ground motion prediction. While the relationships between source parameters described in this paper are significant simplifications of the true complexity of the physics of the rupture process, they help identify important interactions between source properties that are relevant for strong ground motion prediction.

Introduction

Statistical models have long been proposed to characterize heterogeneity in earthquake slip and to relate it to observable characteristics of earthquake ground motion [*Haskell*, 1966; *Aki,* 1967]. *Andrews* [1980b] presented a theoretical formulation for this problem for heterogeneous faults that has formed the foundation for most subsequent efforts [*Herrero and Bernard*, 1994; *Frankel*, 1991; *Zeng et al*., 1994]. *Andrews* [1980b] showed that a two-dimensional slip function $D(x,z)$ with a fractal dimension $D = 2$ results in a far-field spectral decay of displacement as ω^{-2}. The fractal dimension D is related to the wavenumber decay of the two-dimensional Fourier spectrum of the slip function, $D(\boldsymbol{k})$ (where k is the wavenumber); for $D = 2$, the wavenumber spectra decays as $\boldsymbol{k}^{-2}$. Using this relation, *Herrero & Bernard* [1994] propose the "k-square" model that introduces a source-size dependent length scale L_c as well as a wavenumber-dependent behavior of the rise time distribution. *Zeng et al.* [1994] develop the composite source model based on the model of *Frankel* [1991] in which elementary circular sources with a fractal size distribution are summed to form the complete two-dimensional slip function. An explicit assumption in these

models is that stress drop is scale-independent. Moreover, none of these methods directly takes into account slip heterogeneity as imaged using seismic data in finite-source models.

In order to characterize the slip complexity of past earthquakes, *Somerville et al.* [1999] adopt a deterministic approach to correlate the size and number of asperities with seismic moment for a set of finite-source rupture models. *Mai and Beroza* [2002], in contrast, use a spatial random-field model to describe the complexity of earthquake slip distributions. They find that a *von Karman* autocorrelation function for which the correlation length increases with source dimension most closely represents the spectral properties of existing earthquake slip models. Increasing magnitude and hence increasing source dimensions with constant correlation lengths would mean that the rupture would be comprised of many isolated high-slip (high stress-drop) asperities, which would show extremely large slip (and stress drop) in order to accommodate the seismic moment. Unless the correlation length grows with earthquake size, these areas of positive stress drop will be too weakly connected for the rupture to propagate spontaneously because they will be separated by large areas of negative stress drop, and therefore negative elastostatic energy, which will act to stop the rupture.

Guatteri et al. [2002] find that including spatial and temporal variations in slip, slip rise time, and rupture propagation that are consistent with dynamic rupture models exerts a strong influence on near-source ground motion and has the potential to improve strong ground motion prediction. Their results lead to a feasible approach to specify the variability in the rupture time distribution in kinematic models consistently with dynamic source properties. *Mai et al.* [2001] and *Guatteri et al.* [2002] calculate ground motion from a "first-generation" set of pseudo-dynamic models, demonstrating the potential of such a procedure. In this paper, we focus on the generation of the source models by expanding and improving upon the previous "first-generation" pseudo-dynamic source characterization, and leave the ground motion calculation for future applications.

Pseudo-Dynamic Source Characterization

In this paper we define as a *pseudo-dynamic* source model a kinematic model in which the relevant source parameters (slip, rupture velocity and slip-velocity function) are specified in such a way that they emulate both slip distributions of past earthquakes and the temporal behavior of spontaneously propagating dynamic rupture models. We developed the pseudo-dynamic approach (henceforth abbreviated as *PD*) by investigating the relationships between kinematic and dynamic source parameters for a set of dynamic rupture models representing strike-slip earthquakes with a magnitude range of $6.4 < \mathbf{M} < 7.2$.

The complexity of the spatial slip distribution in our *PD* models is characterized as a spatial random field [*Mai and Beroza*, 2002] that is stochastically consistent with slip models for past earthquakes. The starting point of the *PD* model consists of generating a spatial distribution of slip as a realization of a spatial random field.

The characterization of the temporal slip evolution in finite-source rupture models for past earthquakes is limited by a lack of resolution of the variability of temporal slip parameters, such as rupture velocity and slip rise time. The fundamental idea of our approach is that we can overcome this limitation by assuming that dynamic rupture modeling can provide physical constraints to the temporal slip evolution characterization, given a spatial slip distribution. We therefore perform spontaneous dynamic rupture simulations to develop the relationships between kinematic and dynamic rupture parameters to constrain the temporal rupture characteristics. The following section describes our dynamic modeling approach and the various steps toward defining physically consistent rupture velocity, rise time and slip-velocity functions.

Initial Dynamic Rupture Modeling

The first *PD* source characterization was developed by *Mai et al.* [2001] and improved by *Guatteri et al.* [2002]. Both their results were based on the set of 6 stochastic-dynamic models

developed by *Guatteri et al.* [2003] computed using a Boundary Integral Method [*Boatwright and Quin*, 1986; *Das and Kostrov*, 1987; *Quin and Das*, 1989]. These models were discretized into a grid size of 0.75 km, allowing for a maximum frequency of about 2 Hz (for this method), and a slip-weakening fault constitutive relationship was assumed [*Andrews*, 1976; *Day*, 1982] (Figure 1). Table 1 summarizes and defines the relevant dynamic parameters together with a brief explanation of how we assign or calculate them to generate our set of stochastic-dynamic models.

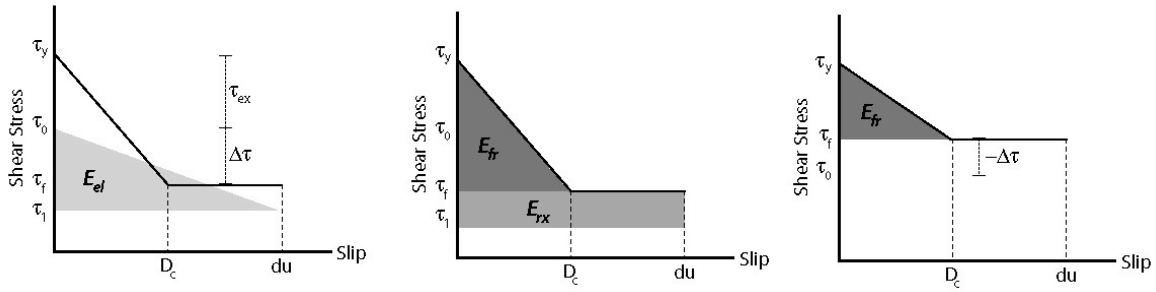

Figure 1: Slip-weakening model showing the relevant energy contributions: elastostatic energy E_{el} (left), fracture energy E_{fr} and relaxation work E_{rx} (center). The right panel displays the case of negative stress drop $\Delta\tau$ for which fracture energy is still defined. See Table 1 for further explanations. τ_1 is the final stress, which may be different from the dynamic frictional level.

TABLE 1: Relevant dynamic parameters

General Information			In this study	
Parameter		Description	Value	Comment
1.	σ_n	Normal stress	150 MPa	Uniform over the fault
2.	μ_d	Coefficient of dynamic friction	0.43	Uniform over the fault
3.	τ_f	Dynamic resistance (frictional stress level)	$\mu_d\sigma_n$	Uniform over the fault
4.	$\Delta\tau$	Stress drop	$\tau_0 - \tau_t$	Calculated from slip distribution (eq. 3)
5.	τ_0	Initial shear stress	$\Delta\tau + \tau_f$	
6.	D_c	Slip-weakening distance	Sampled from [0.25 – 0.4] m for the whole fault	Assigned to lower bound where $\Delta\tau < 0$
7.	E_{fr}	Apparent fracture energy (also termed G_c)	$\frac{1}{2} D_c (\tau_y - \tau_f)$	Simulated from stress drop distribution using (eq. 6)
8.	$\tau_y - \tau_0$	Strength excess τ_{ex}	Calculated from E_{fr} and D_c values	Lower bound $\tau_{ex} = 0.5$ where $\Delta\tau < 0$. Upper bound given by S_{max}
9.	S	Strength parameter	$(\tau_y - \tau_0) / \Delta\tau$	Upper bound $S_{max} = 2.5$
10.	τ_y	Static resistance (upper yield stress)	$\mu_s\sigma_n$	Calculated from (eq. 8) and (eq. 5)
11.	μ_s	Coefficient of static friction	τ_s / σ_n	
12.	E_{el}	Elastostatic energy	$-\frac{1}{2}\, slip_{tot} (\tau_f - \tau_0)$	
13.	E_{rs}	Radiated seismic energy	$E_{el} - E_{fr}$; $E_{rx} = 0$ if the frictional stress τ_f is equal to the final stress τ_1	Assumption: static stress drop is equal to the dynamic stress drop

We assume the same velocity profile as in *Guatteri et al.* [2003] derived from *Boore and Joyner* [1997]. We force the rupture to nucleate at a given hypocenter location and to propagate at a constant rupture speed within a nucleation area whose size is calculated according to *Day* [1982].

Our procedure to generate the new set of stochastic-dynamic models is very similar to that of *Guatteri et al.* [2003]. We first generate our target slip distribution using the method of *Mai and Beroza* [2002], from which we compute the corresponding static stress drop using the method of *Andrews* [1980]. Once we set the hypocenter location, instead of assigning the fracture energy distribution by the *trial and error* procedure as in *Guatteri et al.* [2003], we applied the empirical relationship between fracture energy and stress drop and crack length developed by *Guatteri et al.* [2002]. In a later section in this paper we describe this relationship in detail and discuss how we modified it to satisfy the assumption of sub-shear average rupture velocity over the entire fault plane for the stochastic-dynamic models.

The set of stochastic-dynamic rupture models are representative of strike-slip earthquakes with a magnitude range of $6.4 < \mathbf{M} < 7.2$. Table 1 summarizes the important features of the dynamic parameters, while Figure 2 schematically shows the roadmap of our *PD* procedure development. Table 2 summarizes the parameters used to define a *PD* model.

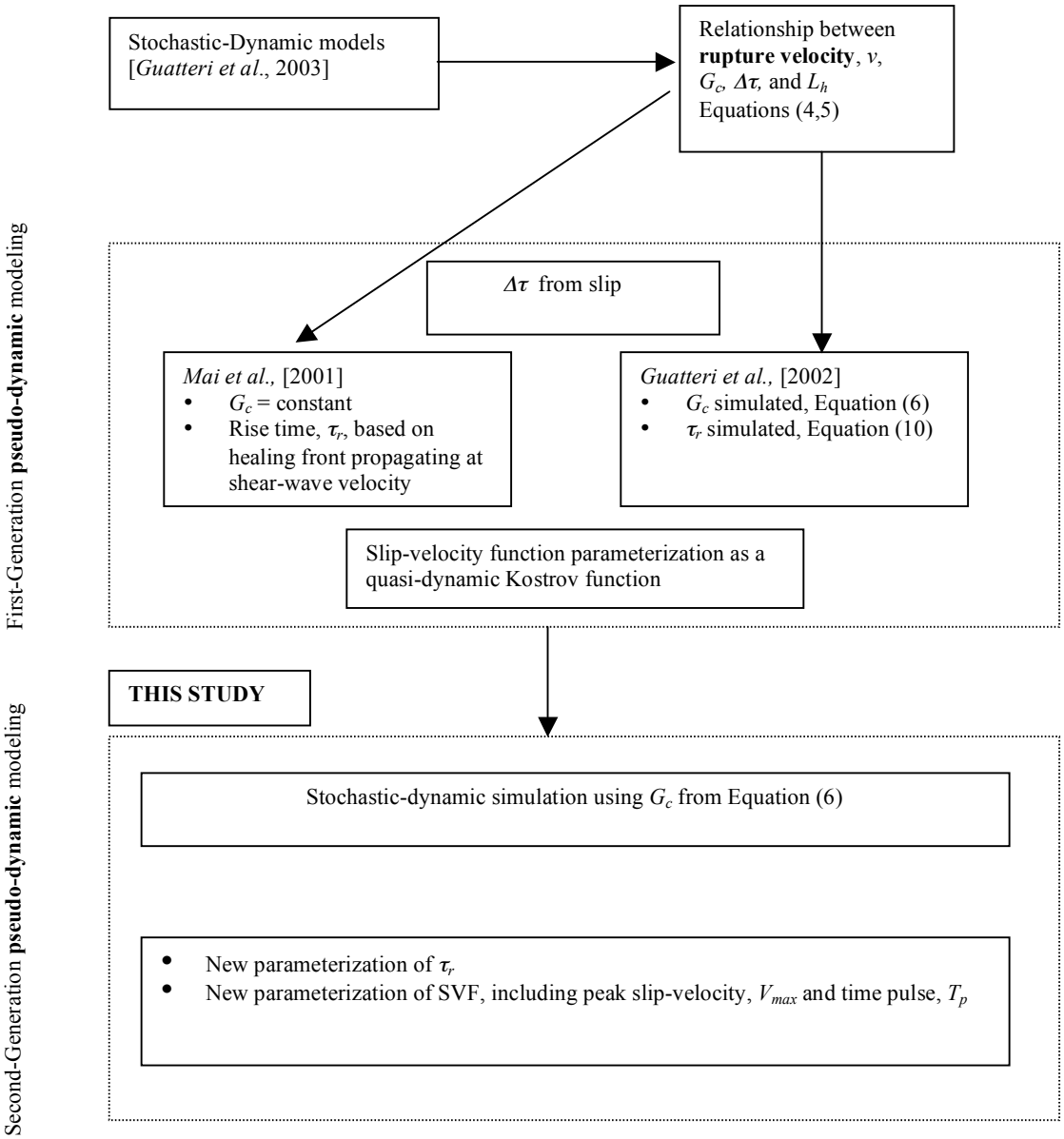

Figure 2: (previous page) Roadmap showing the various phases involved in the development of the pseudo-dynamic procedure presented in this paper.

TABLE 2: Kinematic, dynamic and pseudo-dynamic parameters

Slip	Rupture characteristics	Assigned kinematic parameters
L_h, distance from the hypocenter		
$\Delta\tau$, stress drop	Deduced from kinematic, but not rupture characteristics	Intermediate, dynamic parameters
G_c, fracture energy		
v, rupture velocity	Rupture characteristics	Pseudo-dynamic output parameters
τ_r, rise time		
SVF (V_{max}, T_p)		

Characterization of Spatial Slip Distribution

The variability of slip in earthquakes maps directly into high frequency strong ground motion [*Bernard and Madariaga*, 1983; *Spudich and Frazer*, 1984]. At present, it is not possible to anticipate earthquake slip distributions deterministically, but we can anticipate the characteristics of slip slip variation in earthquakes of a given size if we have a valid stochastic description of the source. With this statistical description of the earthquake source in hand, we can generate many realizations of the slip distribution in a scenario earthquake of interest (with accompanying strong ground motions) without the need to know the slip distribution deterministically.

Here we use a spatial random-field model for earthquake slip to represent the slip distribution [*Mai and Beroza*, 2002], but other models characterizing spatially variable slip are possible [*Andrews*, 1980; *Herrero and Bernard*, 1994; *Zeng et al.*, 1994; *Sommerville et al.*, 1999]. A spatial random field is characterized either in space by its autocorrelation function, $C(r)$, or in the spectral domain by its power spectral density, $P(k)$, where k is the wavenumber. Analyzing a set 44 finite-source rupture models, *Mai and Beroza* [2002] found that a *von Karman* auto-correlation function best represents the power spectral decay of complex earthquake slip, with correlation length increasing with increasing magnitude. The power spectral density $P(k)$ of the *von Karman* auto-correlation function is given by

$$P(k) = \frac{4\pi H}{K_H(0)} \frac{a_x a_z}{\left(1 + k^2\right)^H}, \qquad (1)$$

with $k = \sqrt{a_x^2 k_x^2 + a_z^2 k_z^2}$, H being the Hurst exponent, and K_H the modified Bessel function of the first kind (order H). The characteristic scale lengths are given by the correlation lengths, a_x and a_z in the along-strike and down-dip directions. The Hurst exponent, H, in the expression for the *von Karman* distribution describes the spectral decay at high wavenumbers. The spectral

decay of 44 source models studied by *Mai and Beroza* [2002] revealed that $H = [0.8 – 1.0]$, and that the correlation length scale with magnitude as:

$$a_x \approx 2.0 + \tfrac{1}{3} L_{eff} \qquad log(a_x) \approx -2.5 + \tfrac{1}{2} M_w$$
$$a_z \approx 1.0 + \tfrac{1}{3} W_{eff} \qquad log(a_z) \approx -1.5 + \tfrac{1}{3} M_w \tag{2}$$

where L_{eff}, W_{eff} are the effective source dimensions as defined in *Mai and Beroza* [2000].

We generate heterogeneous slip distributions for the selected target earthquake magnitudes using equations (1) and (2). Source dimensions for these earthquakes ($6.4 < \mathbf{M} < 7.2$) are calculated following *Mai and Beroza* [2000]. Having calculated the power-spectral density $P(k)$, the two-dimensional slip function is obtained by assuming a uniform-random phase and subsequent two-dimensional Fourier transformation under the requirement of Hermitian symmetry to ensure a purely real valued slip-function.

Calculating Static Stress Drop from Slip Distribution

The complete stress-time history can only be calculated by knowing the entire slip-time evolution of the rupture [e.g., *Bouchon*, 1997]; however, the goal in this study is to define a dynamically consistent slip-time evolution based on the final slip only. For this purpose we use the static stress drop, $\Delta\tau$, associated with slip occurring on the rupture plane, as a fundamental parameter for characterizing the temporal slip evolution. We relate slip and stress to one another by a convolutional integral [*Andrews*, 1980] expressed as a multiplication in the wavenumber domain, as:

$$\Delta\tau(\mathbf{k}) = - K(\mathbf{k}) \cdot D(\mathbf{k}) \tag{3}$$

where $\tau(\mathbf{k})$ and $D(\mathbf{k})$ denote the Fourier transforms of the two-dimensional stress drop $\Delta\tau(x,z)$ and slip-function $D(x,z)$, respectively. $K(\mathbf{k})$ represents the static stiffness function that for crustal rocks can be approximated as $K(\mathbf{k}) = -\tfrac{1}{2}\, \mu\, \mathbf{k}$. Hence, having simulated a two-dimensional slip distribution $D(x,z)$, equation (3) can be used to compute the associated static stress drop $\Delta\tau(x,z)$ by means of Fourier transformation of $D(x,z)$ and subsequent inverse Fourier transformation of $\tau(\mathbf{k})$.

Characterization of Fracture Energy for Temporal Slip Evolution

The characterization of fracture energy G_c is the critical step in our *PD* procedure for determining the temporal evolution of slip. Our *PD* approach is built on the following relationship derived by *Andrews* [1976] for a simple homogeneous anti-plane crack:

$$1 - v^2/\beta^2 = \pi^2 \cdot (R_c / 2)^2, \tag{4}$$

where R_c is the dimensionless parameter:

$$R_c = \mu \cdot G_c / (\Delta\tau^2 \cdot L_h), \tag{5}$$

v is the rupture speed, β is the shear wave speed, μ is the shear modulus, $\Delta\tau$ is the stress drop, and L_h is crack length. *Guatteri et al.* [2003] showed that relationship (4) applies approximately to 3-

D heterogeneous dynamic models suggesting that rupture velocity variability can be inferred from the distribution of dynamic parameters over the fault plane.

Rupture Velocity. The first step towards a temporal slip evolution characterization is to determine a distribution of rupture velocity that is physically consistent with a given slip realization. Given a slip distribution, Equation (4) allows us to achieve this by determining the corresponding stress drop distribution (Equation 3), calculating the crack length L_h which we take as the distance of each point on the fault to the hypocenter, and based on that, generating a physically consistent distribution of fracture energy, G_c.

Fracture Energy. Different distributions of fracture energy may be consistent with a given slip distribution and rupture propagation. Through a trial and error procedure *Guatteri et al.* [2003] imposed the fracture energy distribution on their stochastic-dynamic models such that the resulting rupture velocity would be sub-shear on average everywhere over the fault plane. In order to avoid this time consuming trial and error approach, *Guatteri et al.* [2002] used their set of stochastic-dynamic models to build an empirical relationship to generate a distribution of fracture energy from a given slip model and hypocenter location. After some data exploration they developed an empirical relationship based on the normal linear model where the conditional expectation of G_c is:

$$E(G_c|\boldsymbol{\beta}, \Delta\tau, L_h) = \beta_0 + \beta_1 \Delta\tau L_h^{1/2}, \tag{6}$$

where $\boldsymbol{\beta}$ is the vector containing β_0 and β_1, the regression coefficients that they determined through a least squares regression procedure.Figure 3 shows the fracture energy plotted as a function of the respective predictor $\Delta\tau L_h^{1/2}$ (that is proportional to the stress intensity factor) for all points over the fault plane for all the different dynamic models developed by *Guatteri et al.* [2002].

Relationship (6) can be used either to assign a fracture energy distribution to compute spontaneous rupture models and to apply Equation (5) to calculate a distribution of rupture velocity in our *PD* procedure. Before using it for the latter application, we validated and modified it as described below.

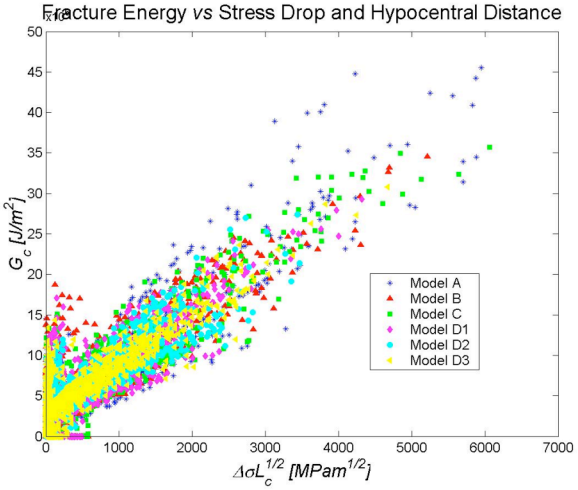

Figure 3: Fracture energy values as a function of stress drop and crack distance. Values relative to different dynamic models described in *Guatteri et al*. [2003] are shown in different colors.

We first applied Equation (6) to derive a distribution of fracture energy to compute a new set of stochastic-dynamic models. However, unlike *Guatteri et al.* [2003], in this study we allow the dynamic models to have areas of negative stress drop (Figure 1). This difference implies that on

average we need lower values of G_c to maintain a sub-shear rupture velocity over the fault plane, because the negative stress drop areas increase the resistance of the fault to rupture. As a result, we find that lower values of regression coefficients β_0 and β_1 are needed than those found previously by *Guatteri et al*. [2002].

Furthermore, we found that two distinct sets of coefficients are needed, corresponding to rupture models with **M** <= 6.5 and for **M** > 6.5, respectively. The two sets are $\beta_0 = 0.18$ and $\beta_1 = 0.0015$ for **M** <= 6.5, and $\beta_0 = 2.7$ and $\beta_1 = 0.0021$ for **M** > 6.5. The difference β_0 stems from the difference in average stress drop values, while the almost identical slope β_1 indicates that the dependency of the stress intensity factor is preserved. We interpret this result as a consequence of lower stress drop values in our rupture models with **M** <= 6.5 than those with a larger magnitude, with corresponding different values of available elastostatic energy E_{el} (Figure 1, Table 1). This would imply that the coefficients of the fracture energy distribution in Equation (6) vary as a function of earthquake magnitude.

The possibility that the scaling coefficients for fracture energy G_c are different for earthquakes below and above **M** = 6.5 has interesting implications as this is the magnitude range where standard scaling relations may break down [*Shimazaki*, 1986; *Hanks and Bakun*, 2003]. Once rupture width approaches the thickness of the seimogenic zone, and rupture length L becomes larger than about twice rupture width W, ruptures grow in along-strike direction only, and the above defined crack length L_h becomes progressively larger for larger/longer earthquakes, requiring higher values of fracture energy G_c

Equation (6) is derived for points on the fault having a positive stress drop. For areas of negative stress drop, we assign a constant value of G_c calculated as the area shown in Figure (1c) by assuming minimum allowed strength-excess and D_c values (Table 1). Note that the use of Equation (6) provides a very simplistic parameterization of fracture energy given a slip distribution (and therefore a static stress drop distribution) and hypocenter. The resulting fracture energy distribution represents only one possible realization out of the space of physically plausible fracture energy distributions consistent with a given slip model. However, Equation (6) contributes to the intent of this paper to provide a simple tool to quickly generate a physically consistent rupture model.

Having assumed in our dynamic models distributions of D_c and strength excess that are fairly uniform and within assigned limits, the strong dependency of G_c on stress drop in our modeling appears to be an artifact of our assumptions. As pointed out by *Favreau and Archuleta* [2003], however, it is plausible that larger values of stress drop are necessary to break stronger barriers of energy, or else the rupture would stop. The dependency found between G_c and the stress intensity factor may be physically interpreted as corresponding to the increase of energy lost due to the occurrence of off-fault microcracking with rupture propagation distance [*Andrews*, 1976; *Peck et al*., 1985].

Slip-Velocity Function Parameterization

A realistic parameterization of the slip-velocity function (SVF) is a critical component of earthquake rupture modeling for strong motion prediction. As for the rupture velocity, the variability of the SVF is poorly constrained from waveform inversion procedures. In dynamic modeling the shape of the SVF at different fault points depends on several factors, such as local stress parameters and distance from the hypocenter [*Day*, 1982; *Nakamura and Miyatake*, 2000; *Guatteri and Spudich*, 2000; *Guatteri et al*., 2003]. Typical SVFs of dynamic models governed by a slip-weakening friction law are shown in Figure 4. Despite the considerable complexity seen in these slip-velocity functions, their time-dependence shows an approximate $t^{-1/2}$–decay, consistent with the quasi-dynamic Kostrov-type slip-velocity function proposed by *Archuleta and Hartzell* [1981]. Note that some points on the fault are characterized by a long tail of low slip-

velocity. From inversion of strong-ground motion, it is not clear whether such low-amplitude tails would be resolved.

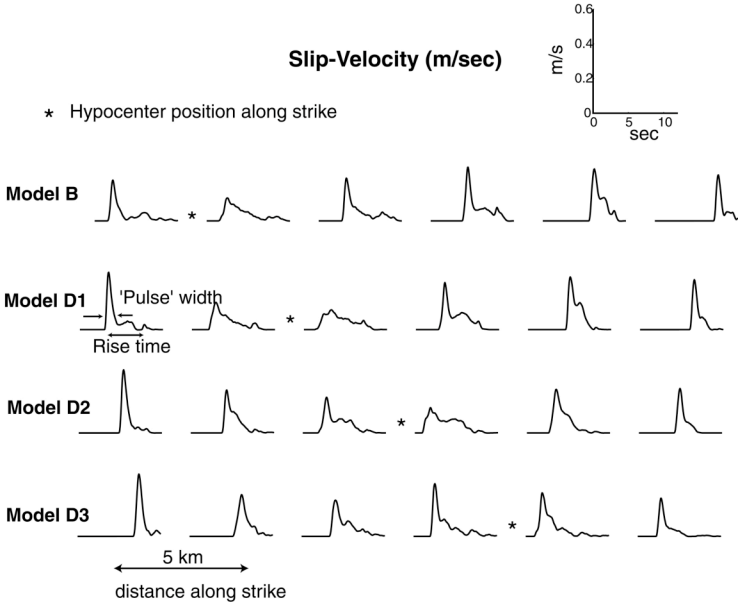

Figure 4: Slip-velocity functions for identical points on the fault (each column) at a depth of 9.5 km for four spontaneous-dynamic rupture models [*Guatteri et al*, 2003].

In this study, we define the rise time as the time from 5% to 95% of the total slip, i.e. being representative of the total slip duration. A comparison between the rise time inferred for real earthquakes from kinematic inversion procedure [*Wald et al*. 1994; *Beroza and Spudich*, 1988; *Cotton and Campillo*, 1995] and the rise time defined for dynamic SVF's may not be very meaningful. In order to characterize the shape of the SVF (impulsive vs. smooth), we define an additional time parameter, the 'time pulse' *Tp*, as the time from 5% to 50% of the total slip. For very spiky SVF, *Tp* will be much shorter than for a broad and smooth SVF, while the respective rise time may be of comparable size. We believe that *Tp* is a more relevant time parameter for strong-ground motion prediction than the rise time, particularly at high frequencies

In this study we propose a very simple approximation of the dynamic SVF using a small number of parameters in order both to provide a feasible parameterization within the *PD* procedure and to capture the relevant characteristics of the dynamic SVF for strong-ground motion prediction. *Nakamura and Miyatake* [2000] proposed a SVF parameterization that closely resembles the SVF obtained in dynamic modeling; their characterization is perhaps superior to our proposed approximation, but it is also rather complex to implement within our approach. *Day* [1982] also proposed very insightful relationships between source parameters describing the SVF in dynamic models. We make use of both the *Day* [1982] and the *Nakamura and Miyatake* [2000] results in formulating our parameterization. Table 2 lists the parameters defining the SVF at a given point on the fault: the maximum slip-velocity value V_{max}, the time pulse T_p, and the rise time τ_r.

Figure 5 shows our proposed parameterization of the SVF as a simple approximation of the SVF typical of dynamic models governed by a slip-weakening friction law (Figure 4). The SVF is composed of two overlapping triangles, T1 and T2 with a total base equal to the rise time, τ_r. T1 is an isosceles triangle having an area A equal to half of the local total slip S, height equal to V_{max} and base equal to the pulse width T_p. T1 is the portion of the SVF that contributes the most to the seismic radiation. T2 is a rectangular triangle with height equal to $V_2 = cV_{max}$. The area of the non-overlapping part of T2 is equal to A. In this study we set c = ½, but other values may be

chosen. For simplicity, let us assume that slip starts at $t = t_1 = 0$. By solving the following system:

$$\begin{cases} cV_{\max} = \left(-2V_{\max} \big/ T_p\right) t + 2V_{\max} \\ t = t_2 \end{cases} \tag{7}$$

we find t_2:

$$t_2 = T_p(1 - c/2), \tag{8}$$

and for $V_2 = \frac{1}{2} V_{max}$ it follows that $t_2 = \frac{3}{4} T_p$.

The following system of equations applies to our SVF parameterization (Figure 5):

$$\begin{cases} \frac{1}{2} V_{\max} T_p = A \\ A = \frac{1}{2} V_2 (\tau_r - t_2) - \frac{1}{2} V_2 (T_p - t_2) \end{cases} \tag{9}$$

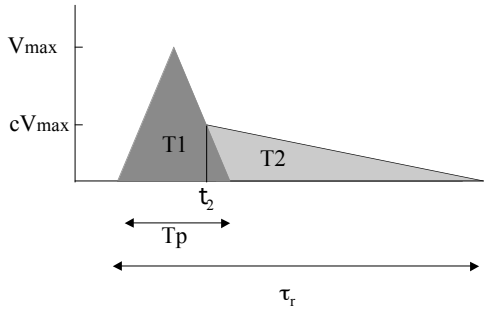

Figure 5. Slip-velocity function parameterization in our *PD* approach, characterized by two overlapping triangles, an isosceles triangle T1 and a rectangular triangle T2.

V_{max}. The value of peak slip-velocity is mainly controlled by the local value of stress drop, of D_c, and distance from the hypocenter [*Day*, 1982; *Andrews*, 1985; *Ohnaka and Yamashita*, 1991; *Nakamura and Miyatake*, 2000; *Guatteri and Spudich*, 2000]. Because for a given stress drop distribution, different choices of D_c result in different peak-slip velocities (a small D_c results in a large V_{max}, and a large D_c in a low V_{max}) [*Guatteri and Spudich*, 2000], we cannot provide a unique parameterization for V_{max} for a given slip distribution. However, the user has the option to set a value of D_c within a given range and tune the SVF shape in a manner consistent with the frequency band of interest in ground motion simulation.

The analysis of our set of dynamic models suggests that the following relationship, modified from *Day* [1982], for V_{max} provides an adequate description of the V_{max} distribution observed in dynamic models:

$$V_{\max} = 0.5 V_{\max \mathrm{Re}\, f} W \tau_p \, v/(\beta\mu), \tag{10}$$

where W is the width of the fault, $\tau_p = \max(\Delta\tau, w(\tau_s - \tau_d))$ and $V_{maxRef} = 0.9\, D_c f_c$, where D_c is a chosen value of slip-weakening distance, $\tau_s - \tau_d = 2G_c/D_c$, and f_c is a frequency parameter defined in *Ohnaka and Yamashita* [1989]. The equation for V_{maxRef} has been adapted from

Ohnaka and Yamashita [1989]. Our definition of τ_p is based on the idea that, if the value of strength excess is very high compared to the stress drop, then it has a large effect on V_{max}. In our parameterization, we found that $w=0.6$ for areas with $\Delta\tau > 0$ and $w=1$ for areas with $\Delta\tau <= 0$ gives a satisfactory fit with the V_{max} distribution of the dynamic models.

Pulse width T_p. As Figure 4 shows, short values of T_p correspond to large values of V_{max}. Figure 6 displays the relationship between T_p and the value of total slip S divided by V_{max} for the points on the fault with a slip and slip-velocity larger than 50% of the maximum slip and maximum slip-velocity over the fault, respectively. A linear relationship provides a simple parameterization of a T_p given V_{max} and the total slip:

$$T_p = \beta_1 S / V_{\max}, \tag{11}$$

where $\beta_1 = 0.84$. Let V_{ave} be the average slip-velocity during T_p, then $0.45\ S = V_{ave}\ T_p$, implying that $V_{ave}\ T_p \approx 1/2 \cdot V_{max}\ T_p$ that justifies our parameterization $0.5 \cdot S = 0.5 \cdot V_{max}\ T_p$. Note that this relationship is derived for areas of large slip and slip-velocity that are the areas of the fault with large seismic energy radiation, and hence contribute the most to strong-ground motions.

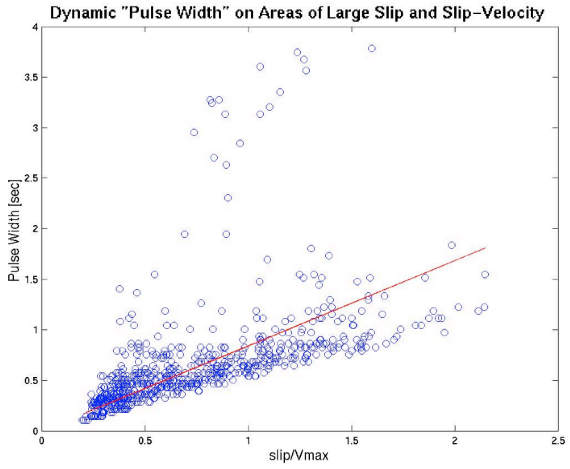

Figure 6. T_p values of the set of 9 dynamic models plotted as a function of the corresponding value of slip/ V_{max}. This plot shows the relationship for the points on the fault having slip and V_{max} values larger than 50% of the maximum slip and slip-velocity, respectively, over the fault.

Slip Rise Time. As for the characterization of the fracture energy distribution, *Guatteri et al.* [2003] built an empirical relationship for slip rise time based on the dynamic models, consistent with our stochastic-dynamic models. Assuming a slip-weakening friction model [*Day*, 1982, *Andrews*, 1985], the duration of slip at a given point on the fault is controlled mainly by the total fault rupture duration. Figure 7 shows the rise time values τ_r plotted as a function of the difference between the total effective fault rupture duration, Tot_{rup}, and the corresponding rupture time value, T_{rup}. The total effective fault rupture duration is the maximum rupture time value among the fault boundary locations aligned with the hypocenter. Figure 7 suggests a normal linear model for an empirical relationship for rise time

$$E(\tau_r|\beta, Tot_{rup}, T_{rup}) = \beta_0 + \beta_1 (Tot_{rup} - T_{rup}). \tag{12}$$

Although we have derived an empirical relationship for τ_r (Equation 12), we require that τ_r be consistent with Equation (9). T_p is one of the most important time parameters in terms of its

influence on the calculated ground motion. Therefore, we follow a 2-step approach to assign all the parameters for SVF such that the consistency with the given slip distribution is satisfied. First, we calculate an initial guess for τ_r from the empirical relationship for the purpose of imposing an upper bound to T_p. Then, from Equation (10), we can solve for τ_r as a function of T_p as follows:

$$\tau_r = T_p + \frac{S}{cV_{\max}}. \tag{13}$$

Figure 8 shows a comparison of *PD* SVF's derived by applying the parameterization described above with the corresponding dynamic SVF's.

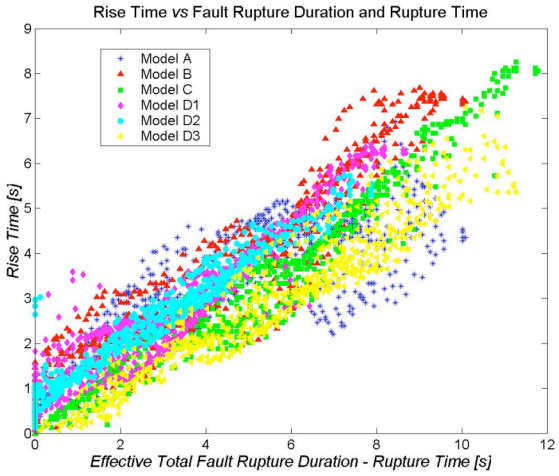

Figure 7. Slip rise time as a function of total fault rupture duration and rupture time. Values corresponding to different dynamic models are shown with different colors.

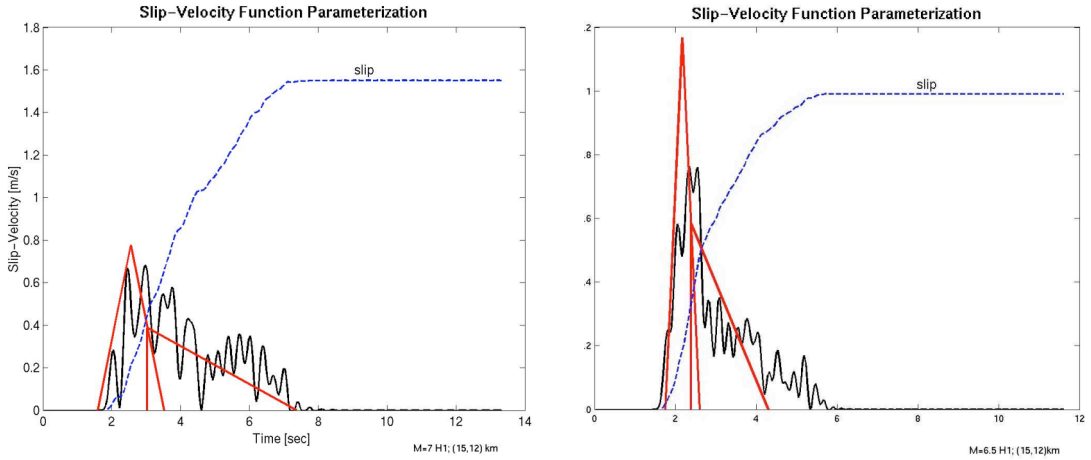

Figure 8. Comparison between the dynamic SVF with the *PD* SVF parameterization proposed in this paper for two selected points on the fault for two different models. The rupture times of the dynamic model has been aligned to that of the *PD* model for better comparison.

Summary of PD-approach:

The basic steps involved in the development of a pseudo-dynamic source realization are the following

1. Define the target earthquake magnitude and event type.
2. Assign or determine the fault dimensions [*Wells and Coppersmith*, 1994; *Somerville et al*, 1999; *Mai and Beroza*, 2000].
3. Set the hypocenter location.
4. Generate a stochastic slip distribution [*Andrews*, 1980; *Somerville et al*, 1999; *Mai and Beroza*, 2002].
5. Compute the corresponding stress drop distribution [*Andrews*, 1980].
6. Generate a distribution of fracture energy (G_c) using Equation (6).
7. Calculate rupture velocity and rupture time distributions using Equation (5).
8. Calculate V_{max} distribution from Equation (10).
9. Apply 2-step procedure to derive the distribution of T_p and τ_r using Equations (11-13).

Figure 9 shows an example of a pseudo-dynamic source model for a M=6.5 strike-slip earthquake. Figure 10 shows a comparison of a fully dynamic source model and its corresponding pseudo-dynamic source characterization. The common constraints to the two source characterizations are the fault geometry, the hypocenter location, the slip distribution and the requirement of sub-shear rupture propagation.

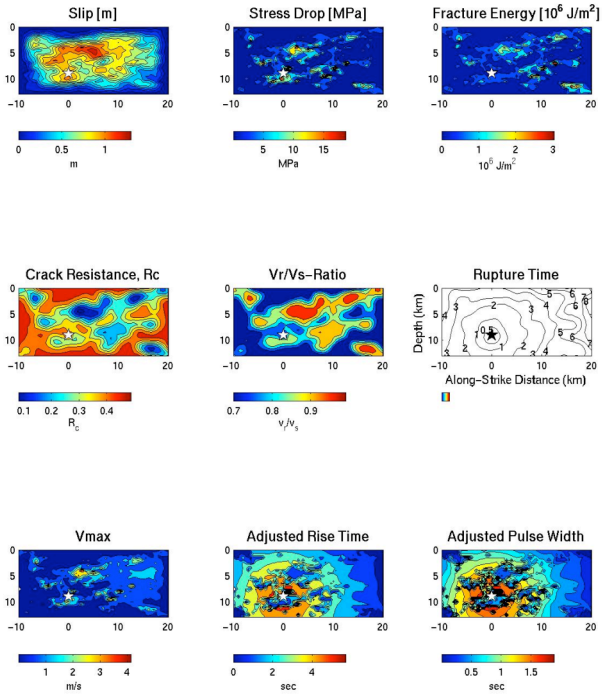

Figure 9. Example representing the *pseudo-dynamic* procedure. The starting point is a slip realization generated as a spatial random field [*Mai and Beroza*, 2002]. The corresponding stress drop distribution is computed using the method of *Andrews* [1980].

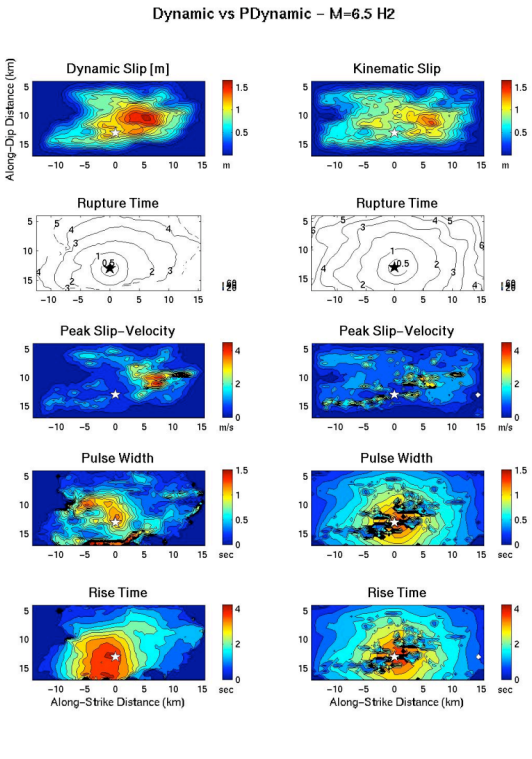

Figure 10. Comparison between a fully dynamic rupture model (left) and a corresponding pseudo-dynamic source model (right). Notice that the main characteristics of the dynamic rupture are represented in the *PD* model, such as the variation in the rupture velocity, the areas with large and low peak slip-velocity, and the areas with short T_p.

Discussion: The energy budget of earthquake rupture

The pseudo-dynamic source characterization developed here is not intended to be a perfect fit to the corresponding spontaneous dynamic rupture models, which are themselves only models of what actually happens in nature during earthquake rupture. The features of the earthquake source most important for realistic strong-ground motion simulations, however, are well described by our *PD* parameterization. The main correlation between source parameters can be described in plain English as follows: the distribution of stress drop is the main factor affecting the distribution of the other dynamic rupture parameters. The rupture velocity correlates with stress drop, V_{max} correlates with stress drop, and T_p and τ_r are inversely proportional to stress drop. Finally, the position of the hypocenter affects the distribution of parameters, and certain hypocenter positions are not plausible as those would not lead to spontaneous rupture propagation. To further investigate this last statement, we analyzed the energy budget during earthquake rupture.

Plausible Models Based on Energy Budget and Hypocenter Location

It is a common and frustrating experience of many dynamic modelers to initiate spontaneous rupture calculations that subsequently abort before rupturing to the desired earthquake size [*Nielsen and Olsen*, 2000; *Oglesby*, 2002; *R. Archuleta*, pers. comm.; *R. Harris*, pers. comm.].

While the investigation of the underlying physical process distinguishing small and large earthquakes is well beyond the scope of this paper, we focus on identifying those target slip distributions that are not consistent with a given hypocenter location based on a simple energy budget calculation. Our approach helped us both to speed up the computation of successful spontaneous rupture models and to select physically plausible (realizable) *PD* models.

In describing the energy budget during earthquake rupture, we follow *Favreau and Archuleta* [2002]. Each point on the fault provides a seismic energy $E_{rs} = E_{el} - E_{fr} - E_{rx}$, where the various terms are defined in Table 1. For simplicity, in this study we neglect the relaxation work E_{rx} spent at the arresting the rupture (Figure 1). As noted by *Favreau and Archuleta* [2002], the fault can be characterized by locally negative seismic energy density values, but its integral on the fault must be positive. Based on this physical requirement, we consider that, as a fundamental condition for its growth, the rupture must be propagating such that the integral of E_{rs} on the rupture area is remains always positive. In other words, while there can be local sinks of energy over the fault, an earthquake process cannot be described overall as a sink of energy. For a given earthquake magnitude, we might expect a more stringent constraint such as a minimum value of radiated seismic energy, but we leave this as an open question for future studies.

It is important to note that the placement of the hypocenter exerts a strong influence on the energy budget as it affects both the specific fracture energy parameterization, as well as the determination of the areas of the fault over which we incrementally integrate E_{rs}. The distribution of elastostatic energy E_{el} can be calculated from the target slip model and the corresponding stress drop. The fracture energy distribution is assigned through Equation (6), and finally the seismic energy density distribution is calculated as shown in Table 1. Although our calculated energy budget strongly depends on our fracture energy parameterization, it provides a consistent approach with our dynamic source modeling and *PD* procedure.

The integrated seismic energy over the ruptured fault area should remain positive in order to allow rupture growth. In other words, if the integrated seismic energy becomes negative, there is no more energy available for the rupture to grow, and hence the rupture would stop. This is the idea proposed originally by *Husseini* [1977] and is consistent with the idea that a small earthquake is like a large earthquake that ran out of energy.

Figure 11 shows the energy budget calculation for a given slip distribution (Figure 11a; the hypocenter location is shown by the star). Figure 11e shows the seismic energy integrated over concentric areas around the hypocenter in order to mimic simplified rupture propagation. Notice that around the hypocenter there is an area that is a large sink of energy. In Figure 11* the

corresponding spontaneous rupture model with identical stress drop and G_c distributions is consistent with the lack of available energy necessary to maintain a rupture growth beyond the nucleation area where the rupture is forced. Figure 12 shows the energy budget calculation for the same slip distribution but a different hypocenter. This model results in a positive integrated seismic energy over the entire fault and is consistent with the rupture propagating over the entire fault (Figure 12*). The same result may be achieved by lowering the G_c, and this approach could be used to test the space of G_c and hypocenters consistent with a given slip distribution, especially before running spontaneous rupture models.

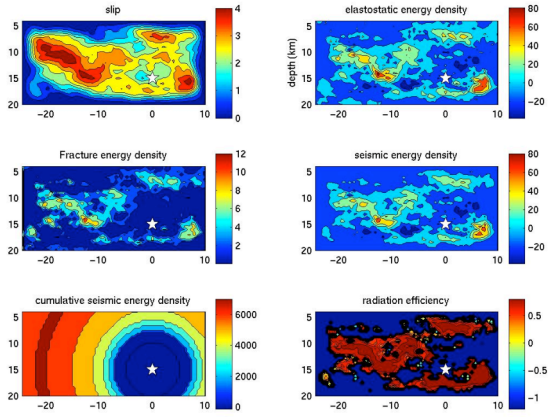

Figure 11. Simulated slip distribution for a M=7 strike-slip earthquake (top left) and the corresponding energy calculations for the *PD*-model. Note of E_{rs} (bottom left) indicated incomplete rupture propagation.

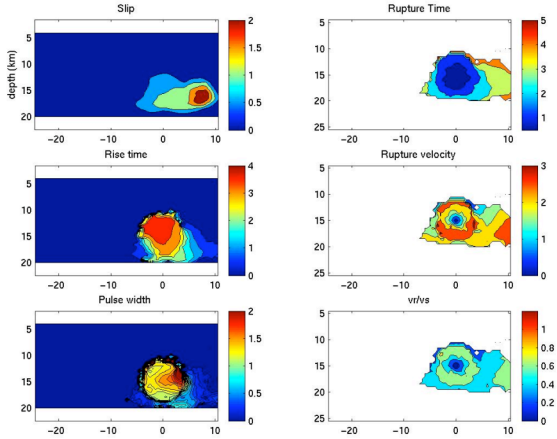

Figure 11*. Dynamic model for the slip distribution shown in Figure 11. Note how the rupture terminated at an early stage, in accordance to what Figure 11 indicates.

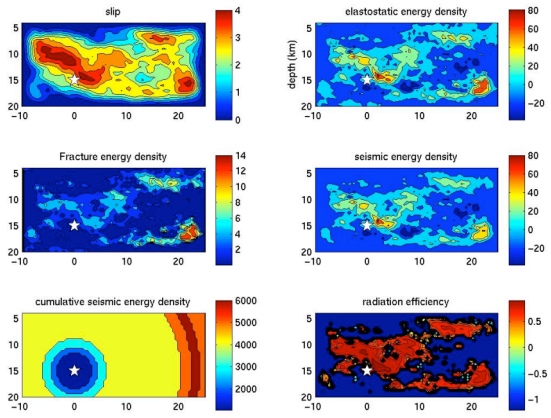

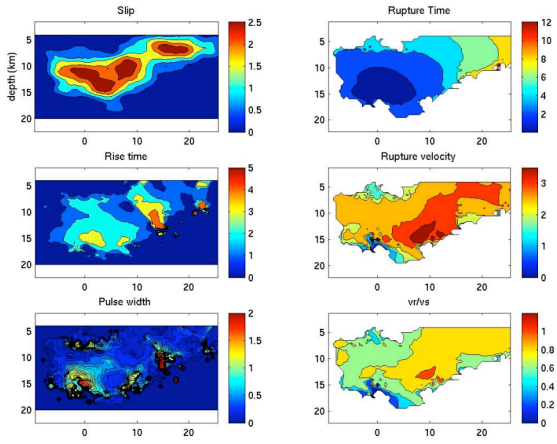

Figure 12. Same slip distribution as shown in Figure 11, but different hypocenter location; the *PD*-energy calculations indicate that the rupture would propagate farther in this case.

mic model for the r
vn in Figure 12. Note th
deed propagated over a
agreement to Figure 1
11.

Conclusions and Caveats

Dynamic rupture modeling has the advantage with respect to kinematic modeling of providing a physically self-consistent earthquake source characterization. *Guatteri et al.* [2003] showed that it leads to a realistic representation of ground motion time histories and to a realistic prediction of ground motion intensity from future earthquakes. In our work we have shown that a pseudo-dynamic source characterization has the potential to improve the source model design (physically based) in probable earthquake scenarios. Pseudo-dynamic modeling is a feasible approach for the simulation of suites of ground motion time histories, merging naturally with the probabilistic approach usually taken for seismic hazard analysis. However, the *pseudo-dynamic* procedure outline above has focused on strike-slip earthquakes in the magnitude range from 6.4 to 7.2. Future work will be devoted to investigate and develop a *PD*-model that also includes dip-slip earthquakes, and is potentially applicable over a wider magnitude range. At the time of writing this report, we have only limited experience in applying the *PD*-approach to large-magnitude earthquakes [*Mai et al*, 2001] that already suggest that at least size-dependent relationships for the fracture energy G_c should apply. The application of our *PD*-model to earthquake scenarios that are clearly out of the range for which the current characterization has been developed warrants extra care and validation of the results.

References

Abrahamson, N. A. and W. J. Silva (1997). Empirical response spectral attenuation relations for shallow crustal earthquakes, *Seism. Res. Lett*. 68, 94-128.

Aki, K., Scaling law of seismic spectrum, *J. Geophys. Res.,* 72, 1217-1231, 1967.

Andrews, D.J. (1976). Rupture propagation with finite stress in antiplane strain, *J. Geophys. Res.*, 81, 3575-3582.

Andrews, D.J. (1980). A stochastic fault model, I. Static case, *J. Geophys. Res.*, 85, 3,867-3,877.

Andrews, D.J. (1985). Dynamic plane-strain shear rupture with a slip-weakening friction law calculated by a boundary integral method, *Bull. Seismol. Soc. Am.*, 75, 1-21.

Andrews, D.J. (1999). Can we infer slip-weakening displacement from seismic observations?, Eos Transactions, American Geophysical Union, vol. 80

Arculeta, R.J., and S. Hartzell (1981). Effect of fault finiteness on near-source ground motion, *Bull. Seismol. Soc. Am.*, 71, 939-957.

Bernard, P., and R. Madariaga, A new asympototic method for the modeling of near-field accelerograms, *Bull. Seismol. Soc. Am.*, 74, 539-557, 1984.

Beroza, G. C., and P. Spudich (1988). Linearized inversion for fault rupture behavior: application to the 1984, Morgan Hill, California, earthquake, *J. Geophys. Res.*, 93, 6275-6296.

Boatwright, J. and H. Quin (1986). The seismic radiation from a 3-D dynamic model of a complex rupture process, Part 1. Confined rupture, in *Earthquake Source Mechanics*, S. Das, J. Boatwright, and C. Scholz ed., AGU, Washington, D.C.

Boore, D. M., and W. B. Joyner (1997). Site amplifications for generic rock sites. *Bull. Seism. Soc. Am*. 87, 327-341.

Bouchon M (1997). The state of stress on some faults of the San Andreas system as inferred from near-field strong motion data, *J. Geophys. Res.*, 102 (B6), 11731-11744.

Cotton, F., and M. Campillo (1995). Frequency domain inversion of strong motions: application to the 1992 Landers earthquake, *J. Geophys. Res.*, 100, 3961-3975.

Das. S., and B.V. Kostrov (1987). On the numerical boundary integral equation method for three-dimensional dynamic shear crack problems, *J. Appl. Mech.*, 54, 99-104.

Day, S.M. (1982). Three-dimensional simulation of spontaneous rupture: The effect of nonuniform prestress, *Bull. Seismol. Soc. Am.*, 72, 1,881-1,902.

Gelman, A., J.B. Carlin, H.S. Stern, and D. B. Rubin (1995). Bayesian data analysis. Chapman & Hall, London.

Favreau P, and R.J. Archuleta (2003). Direct seismic energy modeling and application to the 1979 Imperial Valley earthquake, *Geophys. Res. Lett*., 30 (5), 1198-2002.

Guatteri, M., and P. Spudich (2000). What can strong motion data tell us about slip-weakening fault-friction laws?, *Bull. Seismol. Soc. Am.*, 90, 98-116.

Guatteri, M., P. M. Mai, and G. C. Beroza (2002). Dynamic and pseudo-dynamic source characterization for strong ground motion prediction, *Eos Trans. AGU, 83*(47), Fall Meet. Suppl., Abstract S12B-1210.

Guatteri, M., P. M. Mai, G. C. Beroza and J. Boatwright (2003). Strong ground motion prediction from stochastic-dynamic source models, *Bull. Seismol. Soc. Am*., 93, 301-313.

Hanks T.C., and W.H.Bakun (2003). A bilinear source-scaling model for M-log A observations of continental earthquakes, *Bull. Seismol. Soc. Am*., 92 (5)*,* 1841-1846.

Haskell, N., Total energy and energy spectral density of elastic wave radiation from propagating faults, II, a statistical source model, *Bull. Seismol. Soc. Am.,* 56, 125-140, 1966.

Hisada, Y. (2000). A theoretical omega-square model considering the spatial variation in slip and rupture velocity, *Bull. Seism. Soc. Am*. 90, 387-400.

Hisada, Y. (2001). A theoretical omega-square model considering the spatial variation in slip and rupture velocity Part 2: Case for a two-dimensional source model, *Bull. Seism. Soc. Am*. 91, 651-666.

Husseini, M.I. (1977). Energy-balance for motion along a fault, *Geophys. J. Roy. Astr. Soc.*, 49 (3), 699-714.

Husseini, M.I., D.B. Jovanovich, and M.J. Randall (1975). Fracture energy of earthquakes, *Geophys. J. Roy. Astr. Soc*., 43 (2), 367-385.

Ide, S. (2002). Estimation of radiated energy of finite-source earthquake models, *Bull. Seism. Soc. Am*. 92, 2,994-3,005.

Mai, P. M., and G. C. Beroza (2000). Source scaling properties from finite-fault-rupture models, *Bull. Seism. Soc. Am*. 90, 604-615.

Mai, P.M., M. Guatteri, and G. C. Beroza (2001). A stochastic-dynamic earthquake source model for strong-motion prediction: earthquake scenarios on the Hayward-Rodgers-Creek fault system, Eos Transactions, American Geophysical Union, 82, 869.

Mai, P. M., M. Guatteri, G. C. Beroza, and J. Boatwright (2001). Toward a more physical basis for strong-motion simulation, *Seis. Res. Lett*, 72, 273.

Mai, P. M., and G. C. Beroza (2002). A spatial random-field model for complex earthquake slip, *J. Geophys. Res*., 107(B11), 2308, doi:10.1029/2001JB000588.

Nakamura, H., and T. Miyatake (2000). An approximate expression of slip velocity time functions for simulation of near-field strong ground motion, *Zishin* (*Journal of the Seismological Society of Japan*), 53, 1-9, (in Japanese)

O'Connel, D.R., and J.P. Ake (1995). Ground motion analysis for Hoover Dam, *Seismotectonic Report*, 94-1, Bureau of Reclamation, Denver, Colorado.

Ohnaka, M., and T.Yamashita (1989). A cohesive zone model for dynamic shear faulting based on experimentally inferred constitutive relation and strong motion source parameters, *J. Geophys. Res.,* 94 (B4), 4089-4104.

Peck, L., R.C. Nolen-Hoeksema, C. C. Barton, and R. B. Gordon (1985). Measurement of the resistance of imperfectly elastic rock to the propagation of tensile cracks, *J. Geophys. Res*. 90, 7827-7836.

Quin, H.R., and S. Das (1989). A hybrid boundary integral equation method for the computation of source time functions for 3D rupture propagation, *Geophys. J. Roy. Astron. Soc.,* 96, 163-177.

Shimazaki, K. (1986). Small and large earthquakes: The effects of the thickness of the seismogenic layer and the free surface, *Earthquake Source Mechanics, AGU Geophys. Mono*. 37, eds S. Das, J. Boatwright, C. Scholz, Washington D.C., American Geophysical Union, 209-216.

Somerville, P. G., N. F. Smith, R. W. Graves, and N. A. Abrahamson, (1997). Modification of empirical strong ground motion attenuation relations to include the amplitude and duration effects of rupture directivity, *Seism. Res. Lett*. 68, 199-222.

Spudich, P., and L.N. Frazer, Use of ray theory to calculate high-frequency radiation from earthquake sources having spatially variable rupture velocity and stress drop, *Bull. Seismol. Soc. Am.,* 74, 2061-2082, 1984.

Wald, D.J., T.H. Heaton, and K.W. Hudnut (1996). The slip history of the 1994 Northridge, California earthquake determined from strong motion, teleseismic, GPS, and leveling data, *Bull. Seismol. Soc. Am*., 86, 49-70.

Wells, D.J., and K.J. Coppersmith (1994). New empirical relationships among magnitude, rupture length, rupture width, rupture area, and surface displacement, *Bull. Seismol. Soc. Am*., 84, 974-1002.

Yamashita, T., and M. Ohnaka (1991). Nucleation process of unstable rupture in the brittle regime – a theoretical approach based on experimentally inferred relations, *J. Geophys. Res.,* 96 (B5), 8351-8367.